A novel fluorescent probe for real-time imaging of thionitrous acid under inflammatory and oxidative conditions

Ning Zhang [a], Yifei Lu [a], Yong Huang [a], Qing Zhang [a], Jianglin Tan [a], Jianxiang Zhang [a,b,**], Mengyun Yao [a,*], Gaoxing Luo [a,***]

[a] Institute of Burn Research, Southwest Hospital, State Key Lab of Trauma, Burn and Combined Injury, Chongqing Key Laboratory for Disease Proteomics, Third Military Medical University (Army Medical University), Chongqing, 400038, China
[b] Department of Pharmaceutics, College of Pharmacy, Third Military Medical University (Army Medical University), Chongqing, 400038, China

ARTICLE INFO

ABSTRACT

Thionitrous acid (HSNO), a crosstalk intermediate of two crucial gasotransmitters nitric oxide and hydrogen sulfide, plays a critical role in redox regulation of cellular signaling and functions. However, real-time and facile detection of HSNO with high selectivity and sensitivity remains highly challenging. Herein we report a novel fluorescent probe (SNP-1) for HSNO detection. SNP-1 has a simple molecular structure, but showing strong fluorescence, a low detection limit, a broad linear detection range (from nanomolar to micromolar concentrations), ultrasensitivity, and high selectivity for HSNO in both aqueous media and cells. Benefiting from these unique features, SNP-1 could effectively visualize changes of HSNO levels in mouse models of acute ulcerative colitis and renal ischemia/reperfusion injury. Moreover, the good correlation between colonic HSNO levels and disease activity index demonstrated that HSNO is a promising new diagnostic agent for acute ulcerative colitis. Therefore, SNP-1 can serve as a useful fluorescent probe for precision detection of HSNO in various biological systems, thereby facilitating mechanistic studies, therapeutic assessment, and high-content drug screening for corresponding diseases.

1. Introduction

NO and H$_2$S gases are endogenously generated by certain enzymes, and they affect a wide range of physiological and pathological processes [1–4]. Their biological effects can be the same and/or partially interdependent. As a result, various biochemical reactions may occur, which can negate, weaken, or enhance each other [5–7]. Previous studies indicated that the functions of NO and H$_2$S inside our bodies are closely interlinked [8–10]. Therefore, there is increasing interest in exploring the interactions of H$_2$S and NO in living organisms, to further understand the mechanisms underlying various physiological and pathophysiological reactions and processes using effective molecular tools [11,12]. It has been demonstrated that the NO/H$_2$S cross-linking reactions can produce various reactive nitrogen species (RNS), such as nitroxyl (HNO), thionitrous acid (HSNO), nitroso-persulfide (SSNO$^-$),

and S-nitroso-thiols (RSNO) [13,14]. Among them, thionitrous acid (HSNO), the smallest RSNO, has attracted much attention, since it can be used as a NO–H$_2$S signaling molecule [15–17]. HSNO is the initially formed product by NO/H$_2$S crosstalk reactions. Moreover, HSNO can diffuse through cellular membranes quickly, due to its small size, therefore it easily reach intracellular targets [16,18]. Consequently, HSNO can be regarded as a preferred RNS to study the crosstalk between H$_2$S and NO. However, HSNO, formed as a mixture of rapidly interconverting isomers, possesses a high chemical reactivity due to either homolytic or heterolytic bond cleavage [18,19]. Because of its instability, it is highly challenging to develop effective methods for selective and sensitive detection of HSNO [20,21].

To date, different spectroscopic methods, such as UV–visible, Fourier transform infrared, ^{15}N NMR, and electrospray ionization time-of-flight mass spectrometry, have been employed for HSNO detection in the

---

physiological environment [15]. However, these methods cannot be used for real-time detection and cellular imaging. In this regard, fluorescence techniques offer distinct advantages including high sensitivity, convenience, and high spatiotemporal resolution, in combination with microscopy. Analysis of some HSNO-relevant reactions revealed that HSNO has sulfane sulfur character and performs *trans*-nitrosation, similar to other RSNO compounds [22]. This preliminary information on the dual reactivity of HSNO enabled the development of a fluorescent probe (TAP-1) for HSNO detection [23]. TAP-1 is very sensitive and specific to the presence of HSNO, and it demonstrated effectiveness for visualizing cellular HSNO formation in HEK293 cells. However, the synthesis of TAP-1 is a complex and multi-steps procedure, involving multifarious and high cost starting materials. More importantly, the imaging capability of this probe remains to be examined in relevant disease models. To address the above issues, we aim to design a new fluorescence probe with a succinct structure for real-time and precision detection of HSNO in biological systems. HSNO possesses a high reactivity and it can "immediately" decompose into NO• and HS• (Fig. 1A) [15,18,24]. Consequently, NO•, as a part of the HSNO molecule can interact with o-phenylenediamine of SNP-1 to yield a N-nitroso adduct (benzotriazole). Meanwhile, H$_2$S molecules are produced by the nucleophilic substitution reaction, which then reduce the azide group of the probe to an amine (Fig. 1A). Otherwise, SH radicals generated from HSNO homolysis can be transformed into a strong reducing compound H$_2$S$_2$, followed by rapid decomposition into H$_2$S which also can reduce the azide group of SNP-1 [18,25]. Such dual nucleophilic and reducibile characteristics are unique to HSNO. NO, while H$_2$S alone or other RSNO do not exhibit such duality. Therefore, the development of fluorescent probes based on the dual reactivity of HSNO is highly reasonable and feasible. Herein we developed a novel fluorescent probe (SNP-1) for HSNO detection (Fig. 1B). The SNP-1 fluorescence can be completely quenched by the activation of photo-induced electron transfer (PET) to o-phenylenediamine and the blockage of internal charge transfer (ICT) from the azide group [26,27]. As a result, SNP-1 exhibits very low background fluorescence. In the presence of HSNO, the electron withdrawn azide group will be quickly transferred to the electron-donating amine, which removes ICT blocking for the probe. Simultaneously, o-phenylenediamine of SNP-1 will be transformed to a benzotriazole derivative, thereby eliminating the fluorescence quenching effect of PET. The resulting product (SNP-G) exhibits strong fluorescence. In contrast to HSNO, H$_2$S or NO only reacts with either o-phenylenediamine or azide groups, and the resulting products SNP-HS and SNP-NO do not show any significant fluorescence, because the state of the only

one (out of two electrons) is changed during the electron transfer. Also, we speculate that our new probe can be turned on if H$_2$S and NO coexist, which still leads to the HSNO formation. In this aspect, our probe SNP-1 is a very specific molecular sensor to probe HSNO under both physiological and pathological microenvironments.

2. Experimental section

2.1. Materials and instruments

4-Bromo-1,8-naphthalic anhydride, 4-nitrobenzene-1,3-diamine, stannous chloride (SnCl$_2$), sodium azide (NaN$_3$), S-nitrosoglutathione (GSNO), sodium sulfide nonahydrate (Na$_2$S·9H$_2$O), DL-propargylglycine (PAG), aminoguanidine hydrochloride (AG), 5-aminosalicylic acid (5-ASA), D-cystine (D-cys), and cell counting kit-8 were purchased from Sigma-Aldrich (St. Louis, U.S.A.). All solvents were reagent grade. Dextran sulfate sodium (DSS, 35,000 Da) was purchased from MP Biomedical (U.S.A.). Minimum Essential Medium (MEM) was provided by Gibco (Waltham, U.S.A.). Trypsin, penicillin, streptomycin, and fetal bovine serum (FBS) were purchased from HyClone (Waltham, U.S.A.). Reactions were magnetically stirred and monitored by TLC using Merck Kieselgel 60 F^{25}4 plates and visualized under UV light at 254 nm. Column chromatography was performed with silica gel (60–120 mesh size). ^{1}H NMR spectra were obtained on an Agilent 400 MR spectrometer at ambient temperature and reported in ppm downfield from TMS (0 ppm). ^{13}C NMR spectra was obtained with proton decoupling on an Agilent 400 MR DD2 (100 MHz) or 600 MR DD2 spectrometer and reported in ppm relative to DMSO. NMR data were processed by software Mest Re-Nova (Ver. 9.0.0.12821, Mestrelab Research S.L.). High resolution mass spectra were obtained on a Bruker SolariX 7.0 T spectrometer. Confocal micrographs were obtained on a confocal laser scanning microscope (Olympus SpinSR). Fluorescent images of tissues were obtained on an automatic digital slide scanning system (Olympus SlideView VS200).

2.2. Design and synthesis of new fluorescent probe SNP-1

Briefly, the designed fluorescent probe SNP-1 was synthesized by the following steps (Fig. 2A and Figs. S1–S9). First, compound 1 (4-bromo-1,8-naphthalic anhydride, commercial material) was coupled with 4-nitrobenzene-1,3-diamine to form compound 2 [28]. The nitro group of compound 2 was reduced by stannous chloride dehydrate to yield compound 3. The bromine of compound 3 was substituted by the azide group, forming SNP-1. Thus, SNP-1 could be synthesized by a
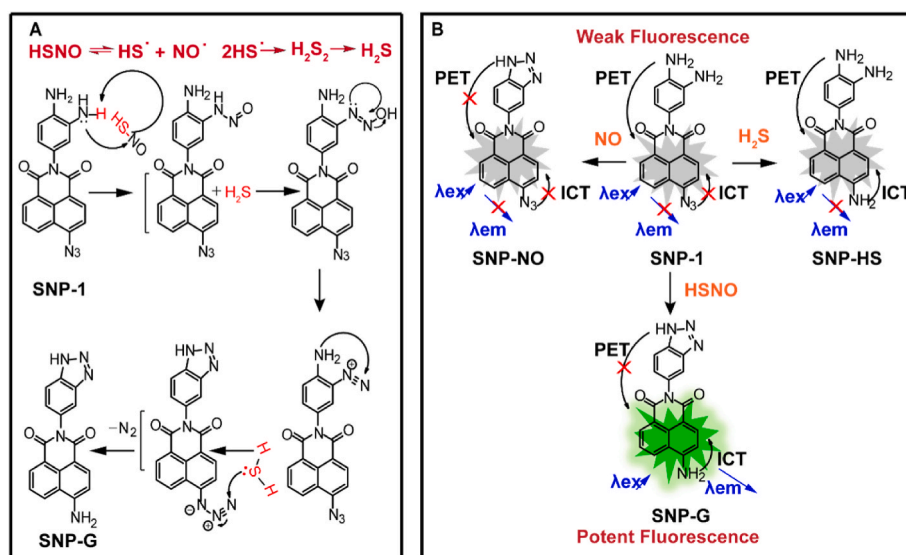

Fig. 1. (A) Design of a HSNO-responsive fluorescent probe SNP-1. (B) Mechanisms underlying the formation of a potent fluorescence compound SNP-G.
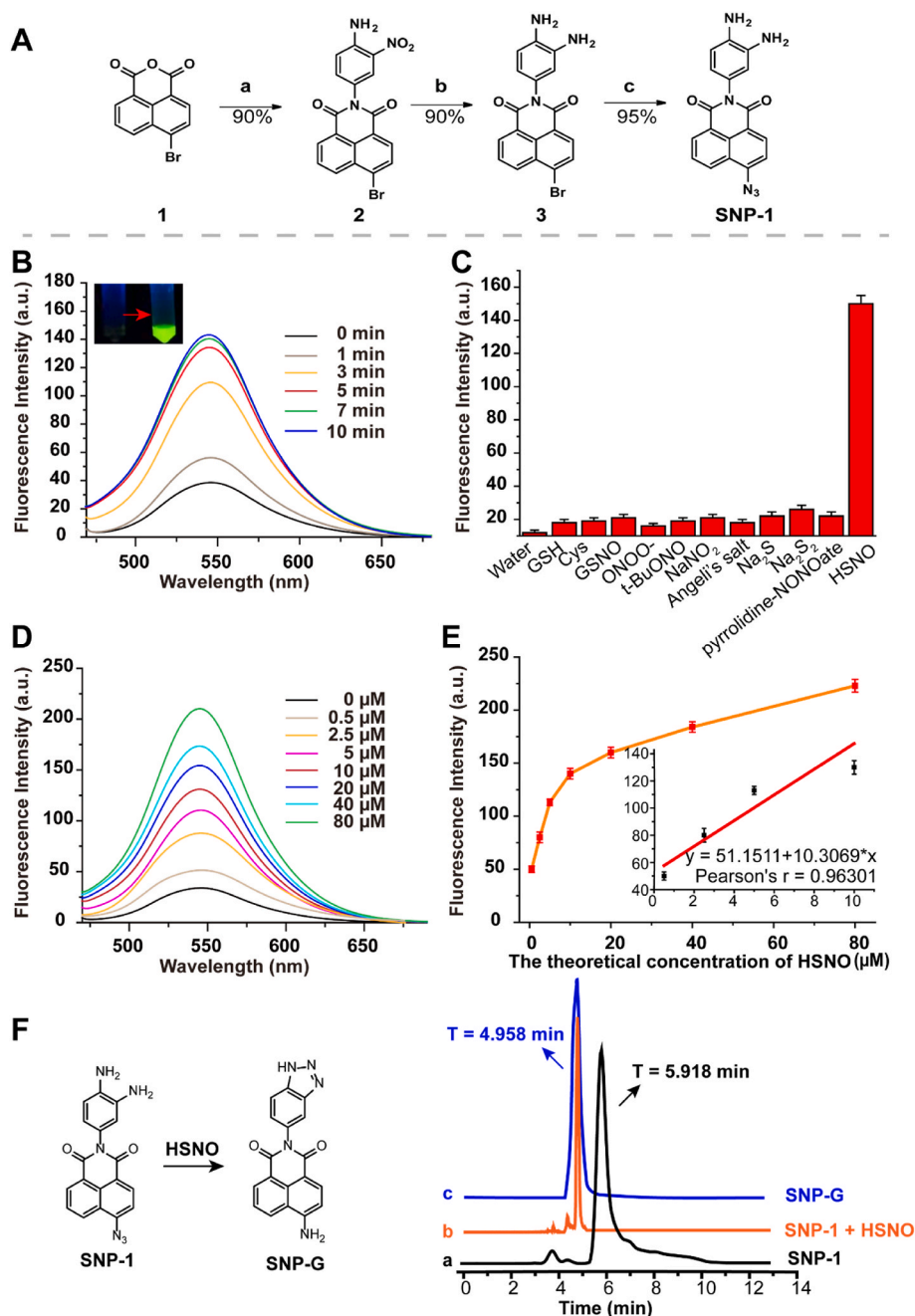
Fig. 2. (A) A synthesis route for SNP-1. **a,** 2-methox-yethanol, 2-Nitrobenzene-1,4-diamine, reflux, 24 h **b,** SnCl$_2$, MeOH, room temperature, 0.5 h **c,** NaN$_3$, DMF, 60 °C, 6 h. (B) Time-dependent fluorescence spectra of 5 μM SNP-1 in the presence of 100 μM HSNO. λ$_{ex}$ = 410 nm. The inset digital photo shows the fluorescence change of SNP-1 before and after the addition of HSNO (UV at 365 nm). (C) Fluorescence intensities of 5 μM SNP-1 at 540 nm in the presence of water alone, 1 mM GSH, 1 mM Cys, 1 μM GSNO, 1 mM ONOO$^-$, 1 mM t-BuONO, 1 mM NaNO$_2$, 1 mM Angeli's salt, 1 mM Na$_2$S, 1 mM Na$_2$S$_2$, 1 mM pyrrolidine-NONOate, and 25 μM HSNO. (D–E) HSNO concentration-dependent fluorescence spectra of 10 μM SNP-1 in PBS at pH 7.4 (D) and quantified fluorescence intensities at 540 nm (E). All spectra were acquired after 10 min of incubation. The inset image in (E) indicates the linear correlation of fluorescence intensities with theoretical HSNO concentrations varying from 0.5 to 10 μM. (F) HPLC curves of SNP-1 (a), 5 μM SNP-1 reacted with 100 μM HSNO (b), and SNP-G (c). The reaction was performed at room temperature for 10 min in 10 mM PBS at pH 7.4 and containing 5% DMSO.

straightforward method involving only three steps, all with high yields, and low cost initial materials.

2.3. Fluorescence measurements

The solutions of various testing species were prepared from glutathione (GSH), cysteine (Cys), Na$_2$S, GSNO, NaNO$_2$, Na$_2$S$_2$, pyrrolidine-NONOate in PBS buffer. The stock solution of Na$_2$S$_2$ was prepared in Deionized water. Peroxynitrite (ONOO$^-$) generation: A mixture of NaNO$_2$ (0.6 M) and H$_2$O$_2$ (0.7 M) was acidified with HCl (0.6 M) and KOH (1.5 M) was added immediately to make the solution alkaline. Manganese dioxide (MnO$_2$) was added and the resulting mixture was stirred vigorously at r. t. for 20 min to remove excess H$_2$O$_2$. The concentration of ONOO$^-$ was determined using the absorption at 302 nm. The stock solution of *tert*-butyl nitrite (t-BuONO) was prepared in ethanol. The stock solution of Angeli's salt were prepared in degassed

10 mM NaOH solution containing 50 μM diethylenetriaminepentaacetic acid (DTPA). The stock solution of HSNO (300 μM) was freshly prepared by mixing 1 mM GSNO and 300 μM Na$_2$S in 50 mM PBS [23]. The stock solution of SNP-1 was prepared in DMSO. All of the test solutions need to be freshly prepared. In a test tube, PBS buffer and the stock solution of cetyltrimethylammonium bromide (CTAB) were mixed, followed by addition of a requisite volume of testing species sample solution. And then added the stock solution of SNP-1. To test the stability of SNP-G, fluorescence spectra of SNP-G (5 μM) in different buffers (pH 5 to 9), at different temperatures (10–60 °C), and with different incubation times (5 min–24 h) were detected. Furthermore, the effects of different compounds, including Na$_2$S (100 μM), GSNO (350 μM), AG (100 μM), and PAG (1 mM), on the fluorescence stability of SNP-G were also examined. The resulting mixture in every test tube was well shaken before scanning the fluorescence spectra of the sample. In the meantime, a blank solution containing no testing species sample was prepared and

measured under the same conditions for comparison.

2.4. High performance liquid chromatography (HPLC) measurement

HPLC was carried out using the Varian 210 HPLC system. A C18 column (Hedera·ODS-2, 5 μm, 250 mm × 4.6 mm) was used with a mixture of acetonitrile and 25 mM of ammonium acetate buffer (8:2, v/v, 1 mL/min, 254 nm) as the mobile phase. The reaction solution of SNP-1 (5 μM) and HSNO (100 μM) in PBS (10 mM, pH 7.4) was measured as the sample.

2.5. Cell culture

The human hepatocellular carcinoma (HepG2) cell line (ATCC HB-8065) were cultured in MEM supplemented with 10% (v/v) FBS, 100 U/mL of penicillin, and 100 mg/mL of streptomycin at 37 °C in a humidified incubator with 95% air and 5% CO_2.

2.6. In vitro cytotoxicity evaluation by CCK-8 assay

Cytotoxicity of SNP-1 was measured with CCK-8 assay. After seeding of HepG2 cells in 96-well plates, cells were allowed to grow 24 h. Then the medium was replaced with fresh medium and SNP-1 (0–60 μM) solutions were added. After 24 h of incubation, cells were washed three times with PBS to remove the excess probe. Culture medium containing 10% CCK-8 (100 μL, v/v) was added into each well. After incubation for 2 h at 37 °C, the plate was taken out from the incubator and put in a plate reader to measure the absorbance of the samples at 450 nm. The cell viability was calculated by comparing the absorbance of the control.

2.7. In vitro fluorescence imaging in HepG2 cells

HepG2 cells were cultured according to the procedures of 2.6 and seeded in 24-well plates. In these experiments, PAG was a H_2S biosynthesis inhibitor and AG was an inducible nitric oxide-synthase blocker. After 70% confluence, cells were treated with SNP-1 or SNP-1 + PAG/AG in FBS-free MEM at 37 °C for 60 min. After removing the excess probe and washing cells with PBS, cells were treated with 100 μM HSNO (in situ generated from GSNO and Na_2S), different concentrations of GSNO (40, 350, 400, and 800 μM) and Na_2S (15, 100, 150, and 300 μM) solutions in FBS-free MEM containing 50 μM CTAB for 30 min at 37 °C correspondingly, and the control groups were treated with FBS-free MEM containing 50 μM CTAB. Cells were then washed with PBS and fixed with 4% paraformaldehyde for 10 min at room temperature, followed by fluorescence imaging under a confocal laser scanning microscope (CLSM). Blue channel of 4',6-diamidino-2-phenylindole (DAPI), was recorded at 410–470 nm with excitation at 360 nm. Green channel of SNP-1 was recorded at 510–570 nm with excitation at 490 nm.

In a separate study, the effects of NO/H_2S sequential treatment on SNP-1 fluorescence in HepG2 cells were examined. To this end, cells were firstly incubated with SNP-1 (50 μM) plus PAG (1 mM) for 60 min, and fluorescence images were recorded. Then cells were treated with 175 μM GSNO for 30 min to acquire fluorescence images. After 60 min of incubation with FBS-free MEM to allow complete GSNO metabolism, cells were treated with 50 μM Na_2S for 30 min, followed by fluorescence microscopy observation. According to similar procedures, cellular fluorescence signals were detected after sequential treatment with H_2S and NO. As a positive control, fluorescence images were recorded after cells were treated with 175 μM GSNO and 50 μM Na_2S simultaneously.

To explore the reactive sensitivity of SNP-1 towards HSNO, cells were incubated with SNP-1 for 30 min, and then treated with various concentrations of HSNO (varying from 0, 0.5, 1, 2, 5, 10, 50, 75, 100, to 150 μM) in FBS-free MEM containing 50 μM CTAB for 30 min at 37 °C, followed by fluorescence imaging by CLSM.

2.8. Animals

The procedures of animal experiments in this study were approved by the Institutional Animal Care and Use Committee of the Third Military Medical University (Chongqing, China). Pathogen-free male BALB/c mice (6–8 weeks old, 19–21 g) were purchased from the Animal Center of the Third Military Medical University and housed in standard cages under standard conditions. All animals were acclimatized for one week before use.

2.9. In vivo biocompatibility evaluation of SNP-1

BALB/c mice (6–8 weeks old, 19–21 g) were administrated with SNP-1 by intravenous injection (50 mg/kg). The mice injected with saline were used as the control group. After administration, the body weight and behaviors of mice were monitored each day. At the predefined time points (24 h and 30 days post administration), complete blood panel analysis and serum biochemistry tests including aspartate aminotransferase (AST), alanine aminotransferase (ALT), UREA, and creatinine (CREA) were conducted using the collected blood samples. Major organs (including heart, liver, spleen, lung and kidney) of rats were weighted for organ index calculation and fixed for histological analysis.

2.10. Fluorescence imaging of HSNO in colon and renal tissues by ex vivo imaging

Pathogen-free 6–8 week old male BALB/c mice were randomly assigned to the Control and HSNO groups. Mice in the control group were intravenously injected with 200 μL of saline and HSNO group mice were intravenously injected with 200 μL of HSNO solution (300 μM, i. v.). After 45 min, both groups were intravenously injected with SNP-1 (10 mg/kg). Two hours later, mice were euthanized and anatomized. Samples of colon and kidney were quickly excised, frozen in liquid nitrogen, embedded in optimal cutting temperature (OCT) cryoembedding medium and subsequently cut into cryosections. Then, the sections were washed with PBS for three times and sealed with sealing liquid containing 4',6-diamidino-2-phenylindole (DAPI) and anti-fluorescent quenching agent, followed by being observed under the automatic digital slide scanning system.

2.11. Establishment of an acute ulcerative colitis model in mice

Acute ulcerative colitis in mice was induced by addition of 3% (w/v) DSS to the drinking water for 7 days [29,30]. On day 1, mice were earmarked for identification. DSS solution was administered to the drinking bottles of the cages (5 mL of DSS solution per mouse per day) while mice in the control group received drinking water without DSS. On day 3 and day 5, bottles were emptied and filled with fresh DSS solution (5 mL of DSS solution per mouse per day), meanwhile, the leftover DSS solution from the bottles were measured to ensure that the changes in colitis activity were not due to the differences in DSS consumption. The weight and disease activity index (DAI) (calculated by body weight decrease, stool consistency and rectal bleeding) [30] were measured and assessed daily throughout the modeling period.

2.12. Establishment of a renal ischemia/reperfusion injury (IRI) model in mice

To establish a renal IRI model, mice were anesthetized (1% pentobarbitone, i. p.) and a heating blanket was used for body temperature maintaining. A tissue separating scissor was used to make a midline laparotomy incision so that an incision of the avascular linea alba was made giving access to the peritoneal cavity and exposing both kidneys. Bilateral renal blood flow was interrupted for 45 min by clamping nontraumatic vascular clamps over renal pedicles. Successful ischemia can be visually confirmed by a gradual uniform darkening of the kidney.

After the period of ischemia, clamps were removed and kidneys would rapidly change color from a dark maroon to a healthy dark pink, which suggesting successful reperfusion. Then intestines were replaced followed by closing the peritoneum with a blanket stitch using 6/0 braided silk suture. Finally iodine solution was applied to the surgical area to minimize the risk of post-operative infection [31,32].

2.13. Study on colonic HSNO in mice with acute ulcerative colitis

Acute ulcerative colitis in mouse was induced by drinking water containing 3% DSS as aforementioned. First, we examined the colonic HSNO levels in mice with colitis. In this case, mice were randomly assigned to four groups: Control, normal mice; Colitis, DSS-induced colitis mice; Colitis + PAG, DSS-induced colitis mice treated with PAG (200 μmol/kg); Colitis + AG, DSS-induced colitis mice treated with AG (2 mmol/kg). PAG (intraperitoneal injection, i. p.) and AG (subcutaneous injection, s. c.) were administered daily during 7 days of DSS treatment. On day 8, all groups were intravenously injected with SNP-1 (10 mg/kg). Two hours later, mice were euthanatized and anatomized. Samples of colon were quickly excised, made into cryosections and observed under the automatic digital slide scanning system as aforementioned.

In another cohort study, mice were randomized to different four groups: Control, drinking water plus oral gavage of saline; Colitis, 3% DSS in drinking water plus oral gavage of saline; Colitis + 5-ASA (L), 3% DSS in drinking water plus oral gavage of 5-ASA (30 mg/kg); Colitis + 5-ASA (H), 3% DSS in drinking water plus oral gavage of 5-ASA (75 mg/kg). 5-ASA was administered daily during 7 days of DSS treatment. On day 8, all groups were intravenously injected with SNP-1 (10 mg/kg). Two hours later, mice were euthanatized and anatomized. Samples of colon were quickly excised, made into cryosections and observed under the automatic digital slide scanning system as aforementioned. Meanwhile, another section of colon tissue was excised from each mouse, fixed with 4% paraformaldehyde and made into paraffin sections for hematoxylin and eosin (H&E) staining.

2.14. Study on renal HSNO in mice suffering from renal IRI

Renal IRI models in mice were established as aforementioned and the renal HSNO levels were examined. In this case, mice were randomly assigned to four groups: Control, normal mice; IRI, mice suffering from renal IRI; IRI + Na₂S, mice suffering from renal IRI administrated with Na₂S (100 μg/kg, i. v.); IRI + AG + Na₂S, mice suffering from renal IRI pretreated with AG (2 mmol/kg, s. c.) and then administrated with Na₂S (100 μg/kg, i. v.). All groups were intravenously injected with SNP-1 (10 mg/kg) 24 h following surgery. Two hours later, mice were euthanatized and anatomized. Samples of kidney were quickly excised, made into cryosections and observed under the automatic digital slide scanning system as aforementioned.

In a separate study, mice were randomized to different four groups: Control, normal mice; IRI, mice suffering from renal IRI; IRI + IPoC, mice suffering from renal IRI treated with ischemic postconditioning (IPoC: immediately after 45 min of ischemia and prior to reperfusion, mice were subjected to 6 cycles of clamping the left renal artery for 10 s of reperfusion after that 10 s ischemia) [33]; IRI + D-cys, mice suffering from renal IRI treated with D-cys (8 mmol/kg, oral gavage). After 24 h, all groups were intravenously injected with SNP-1 (10 mg/kg). Two hours later, blood samples were collected for the examination of serum levels of UREA and CREA. Then mice were euthanatized and anatomized. Samples of kidney were quickly excised, made into cryosections and observed under the automatic digital slide scanning system as aforementioned. Meanwhile, part of kidney tissue was excised from each mouse, fixed with 4% paraformaldehyde and made into paraffin sections for H&E staining.

3. Results and discussion

3.1. In vitro characterization of SNP-1

Fluorescence properties of SNP-1 were tested as in the presence of HSNO. For this purpose, a mixture containing S-nitrosoglutathione (GSNO) and Na₂S (prepared in PBS with pH 7.4) served as an HSNO source [15]. SNP-1 (5 μM) itself showed weak fluorescence emission. When SNP-1 was tested in a HSNO solution (100 μM), notable green fluorescence was observed with the maximal emission wavelength at 540 nm. The fluorescent signal was time-dependent, showing the highest intensity at 7 min (Fig. 2B). The turning on fluorescence could also be directly visualized under UV light (Fig. 2B). Also, fluorescence properties of synthesized SNP-G were separately characterized, showing good quantum yields in different solvents (Table S1). Furthermore, the selectivity of SNP-1 to HSNO was tested by incubation with other reactive compounds, including glutathione (GSH), cysteine (Cys), GSNO, peroxy-nitrite (ONOO⁻), *tert*-butyl nitrite (t-BuONO), NaNO₂, AngeliQs salt (an HNO donor), Na₂S, Na₂SO₃, MCPD (a persulfide donor) [34]. Na₂S₂, Na₂S₃, and pyrrolidine-NONOate (a NO donor) [35]. In this case, only HSNO (in situ generated from GSNO and Na₂S) triggered a notable increase in the fluorescence intensity (Fig. 2C). We also studied the reactive sensitivity of SNP-1 towards HSNO. For this purpose, SNP-1 at 10 μM was incubated with various concentrations of HSNO (the theoretical concentrations of HSNO were calculated based on the concentrations of GSNO and Na₂S). The intensity of SNP-1-derived fluorescence increased gradually as the HSNO content increased (Fig. 2D). Of note, the fluorescence intensity at 540 nm (F540 value) varied from 50 to 220 with the concentration of HSNO changing from 0.5 to 80 μM (Fig. 2E). Moreover, F540 values showed a linear dependence (with the Pearson correlation coefficient r = 0.96301) on the HSNO concentrations varying from 0.5 to 10 μmol/L. Importantly, HSNO quantification with SNP-1 is consistent with the result based on previously reported method (Fig. S10) [36]. Our data suggested that SNP-1 can be utilized to detect HSNO with a detection limit as low as 0.5 μM. Therefore, SNP-1 is potentially adaptive for quantification of trace concentrations of HSNO. In addition, SNP-1 in PBS at various physiological pH values or at different temperatures was proved to be stable, as indicated by negligible fluctuations of fluorescence (Fig. S11). Also, we found similar fluorescence emission spectra for SNP-1 after 10 min of incubation with HSNO at different temperatures (Fig. S12A). Nevertheless, the high temperature could slightly accelerate the transformation of SNP-1 to SNP-G in the presence HSNO (Fig. S12B).

3.2. Mechanisms responsible for HSNO-triggered fluorescence generation of SNP-1

To clarify the reaction triggering the fluorescence generation of SNP-1 in the presence of HSNO, we synthesized SNP-G (acting as a control) and then analyzed SNP-1 reaction with HSNO in situ formed by GSNO and Na₂S using high performance liquid chromatography (HPLC). The data obtained based on this reaction confirmed the transformation of SNP-1 into SNP-G after reaction with HSNO (Fig. 2F). Of note, SNP-G was stable in different solutions, at various temperatures, or after incubation for varied time periods, since the fluorescence intensity showed negligible fluctuations under these different conditions (Figs. S13A–C).

3.3. Imaging of HSNO in living cells by SNP-1

Based on excellent HSNO-responsive fluorescence properties of SNP-1, we then tested it for HSNO imaging in cells. Human hepatocellular carcinoma (HepG2) cells were incubated with 20 μM SNP-1 for 60 min and then rinsed with PBS three times. As expected, strong fluorescence was observed in cells after treatment with HSNO (generated in situ from GSNO and Na₂S) for 30 min (Fig. 3A and B), while under the same
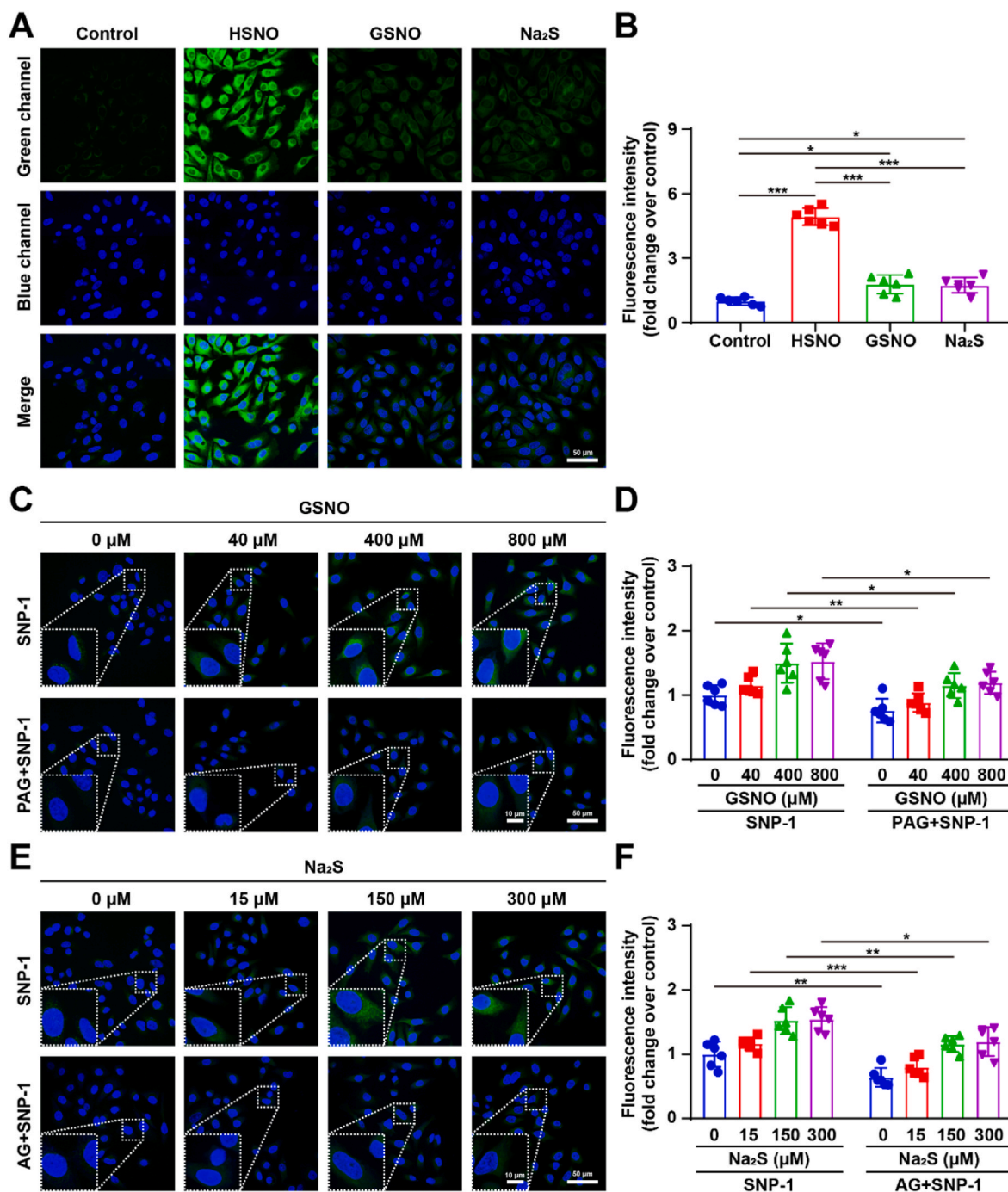
Fig. 3. (A) Confocal micrographs of SNP-1 in HepG2 cells. Cells were incubated with 20 μM SNP-1 for 60 min and treated with FBS-free MEM (Control), 100 μM HSNO, 350 μM GSNO, or 100 μM Na$_2$S for 30 min. (B) The quantified fluorescence intensities. (C) Confocal images of HepG2 cells showing intracellular HSNO generated by the reaction of exogenous NO and endogenous H$_2$S. The cells were incubated with SNP-1 (20 μM) or SNP-1 (20 μM) + PAG (1 mM) for 60 min, then treated with various concentrations of GSNO for 30 min. (D) Quantification of fluorescence intensities. (E) Fluorescence images showing intracellular HSNO generated by the reaction of exogenous H$_2$S and endogenous NO. Cells were incubated with SNP-1 (20 μM) or SNP-1 (20 μM) + AG (100 μM) for 60 min, then treated with various doses of Na$_2$S for 30 min. (F) Quantified fluorescence intensities. Data are expressed as mean ± SD (n = 6). *$p < 0.05$, **$p < 0.01$, ***$p < 0.001$.

conditions, cells treated with either a H$_2$S donor (Na$_2$S) or a NO donor (GSNO and sodium nitroprusside) alone exhibited very low fluorescence signals (Fig. 3A–B, Fig. S14) largely because of their reactions with endogenous H$_2$S/NO, which resulted in the formation of a small number of HSNO molecules. To verify this hypothesis, cells incubated with SNP-1 were treated with the H$_2$S biosynthesis inhibitor propargylglycine (PAG) [37] or the inducible nitric oxide-synthase blocker aminoguanidine hydrochloride (AG) [38] for 60 min, followed by treatment with different concentrations of GSNO or Na$_2$S to produce HSNO in situ.

The fluorescence signal of SNP-1 in PAG pre-treated cells was weaker (Fig. 3C and D). By contrast, fluorescence intensities of cells without PAG pre-treatment notably depended on the GSNO concentration. Similarly, stronger fluorescence was observed in cells without AG pre-treatment, compared to cells pre-treated with AG, while fluorescence in cells without AG pre-treatment was Na$_2$S concentration-dependent (Fig. 3E and F). Moreover, our experimental data confirmed that AG, PAG, Na$_2$S, and GSNO had little influence on the fluorescence intensity of SNP-G (Fig. S13D). The differences in

fluorescence intensities between cells with or without PAG/AG pretreatment indicated the potential intracellular production of HSNO. These results suggested that SNP-1 could detect HSNO in cells. Additionally, SNP-1 could react with intracellular HSNO which was formed by the reaction of exogenous H_2S/NO (derived from Na_2S/GSNO) and endogenous NO/H_2S.

Whereas the above result showed that NO or H_2S alone cannot transform SNP-1 into SNP-G, we further examined the possible effect of sequential treatment with NO/H_2S or H_2S/NO. As shown in Figs. S15–S16, the fluorescence signal of SNP-1 in cells simultaneously treated with GSNO and Na_2S (HSNO formed in this case) was significantly stronger than that of cells sequentially treated with GSNO followed by Na_2S or Na_2S followed by GSNO (without HSNO formation in

both cases). These results suggested that the bright fluorescent signal in cells was mainly triggered by the reaction product of SNP-1 and HSNO. On the other hand, to examine the sensitivity of SNP-1 to HSNO, cells were incubated with SNP-1 for 60 min, followed by treatment with various concentrations of HSNO. It was found that the intracellular fluorescence intensity is proportional to the HSNO concentration (from 2 to 100 μM) in HepG2 cells (Fig. S17). Notably, SNP-1 can be utilized to detect exogenous HSNO in HepG2 cells at a low level of 2 μM. Moreover, the physiological level of HSNO in HepG2 cells could also be detected by SNP-1 (Fig. S18). All these results indicated that SNP-1 can be used to detect HSNO in cells with high sensitivity and specificity.
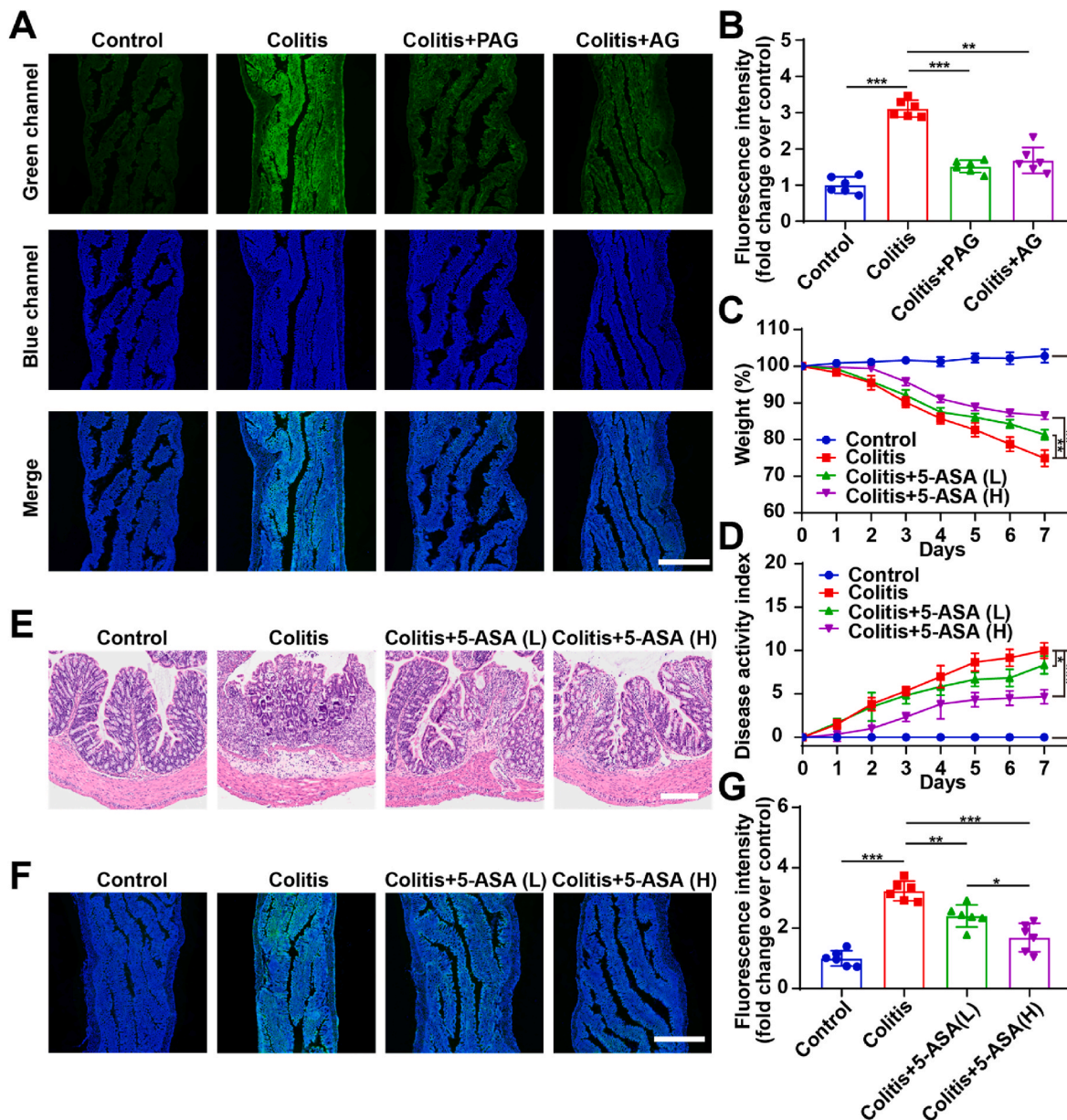

Fig. 4. (A) Representative fluorescence images of colonic sections indicate the increased HSNO level. Control, normal mice; Colitis, DSS-induced colitis mice; Colitis + PAG, DSS-induced colitis mice treated with 200 μmol/kg PAG; Colitis + AG, DSS-induced colitis mice treated with 2 mmol/kg AG. Scale bars, 1 mm. (B) Quantified fluorescence intensities. (C) Changes in the mouse body weight during 7 days of treatment. Data were normalized to the body weight at day 0. (D) The DAI of mice during 7-day treatment. (E) H&E-stained histological sections of colon tissues. Scale bar, 200 μm. (F) Fluorescence images of colon tissues after different treatments. Control, drinking water + oral gavage of saline; Colitis, 3% DSS in drinking water + oral gavage of saline; Colitis + 5-ASA (L), 3% DSS in drinking water + oral gavage of 30 mg/kg 5-ASA; Colitis + 5-ASA (H), 3% DSS in drinking water + oral gavage of 75 mg/kg 5-ASA. Scale bar, 1 mm. (G) Quantitative analysis of fluorescence intensities. Data are presented as mean ± SD (n = 6). *$p < 0.05$, **$p < 0.01$, ***$p < 0.001$.

3.4. Detection of colonic HSNO in mice with acute ulcerative colitis using SNP-1

Generally, impaired NO and H2S metabolism are associated with immune disorders [39,40]. Additionally, high levels of NO and H2S are present in colon tissues from patients with ulcerative colitis and reported to be associated with the occurrence and development of ulcerative colitis [41–43]. Thus, we detected HSNO in colitis mice and determined the changes of HSNO levels along with the course of disease using the newly developed probe SNP-1.

To test the capability of SNP-1 for detecting HSNO in colon tissues, mice were randomly assigned to two groups (Control and HSNO) and intravenously injected with saline and HSNO, respectively. Fluorescence of the HSNO-treated mice showed significantly higher green fluorescence because of the SNP-1 response to HSNO in colon tissues (Fig. S19). Subsequently, we examined imaging capability of SNP-1 in mice with dextran sulfate sodium (DSS)-induced colitis. The fluorescence of the colitis group was 3.1 times higher than that observed for the control group (Fig. 4A and B), which was exactly related to elevated HSNO

levels in the colitis group, since both H2S and NO levels were found to be notably increased (Figs. S20A–B). Additionally, the fluorescence of PAG- and AG -treated groups was only 1.52 and 1.69 times higher than that of the control group, mainly because of lower HSNO levels resulting from the suppressed generation of H2S/NO (Fig. 4A and B). Consistently, decreased H2S levels in PAG-treated group and decreased NO levels in AG-treated group were detected in colon tissues (Figs. S20A–B). All these results revealed up-regulation of HSNO in colon tissues of mice with colitis, which could be controlled by the content of H2S/NO and identified using our new probe SNP-1.

To further demonstrate changes of HSNO levels in colon tissues of mice with different degrees of colitis severity, 5-aminosalicylic acid (5-ASA) was used as a therapeutic agent [44,45]. Colitis mice were induced by DSS and treated with different formulations. Consistent with previous studies [46,47], 5-ASA treatment effectively reduced weight loss (Fig. 4C) and disease activity index (DAI) (Fig. 4D). Besides, examination on hematoxylin and eosin (H&E)-stained sections showed that DSS-induced colitis exhibited significant damages in colon structure with epithelial disruption, goblet cell depletion, and significant
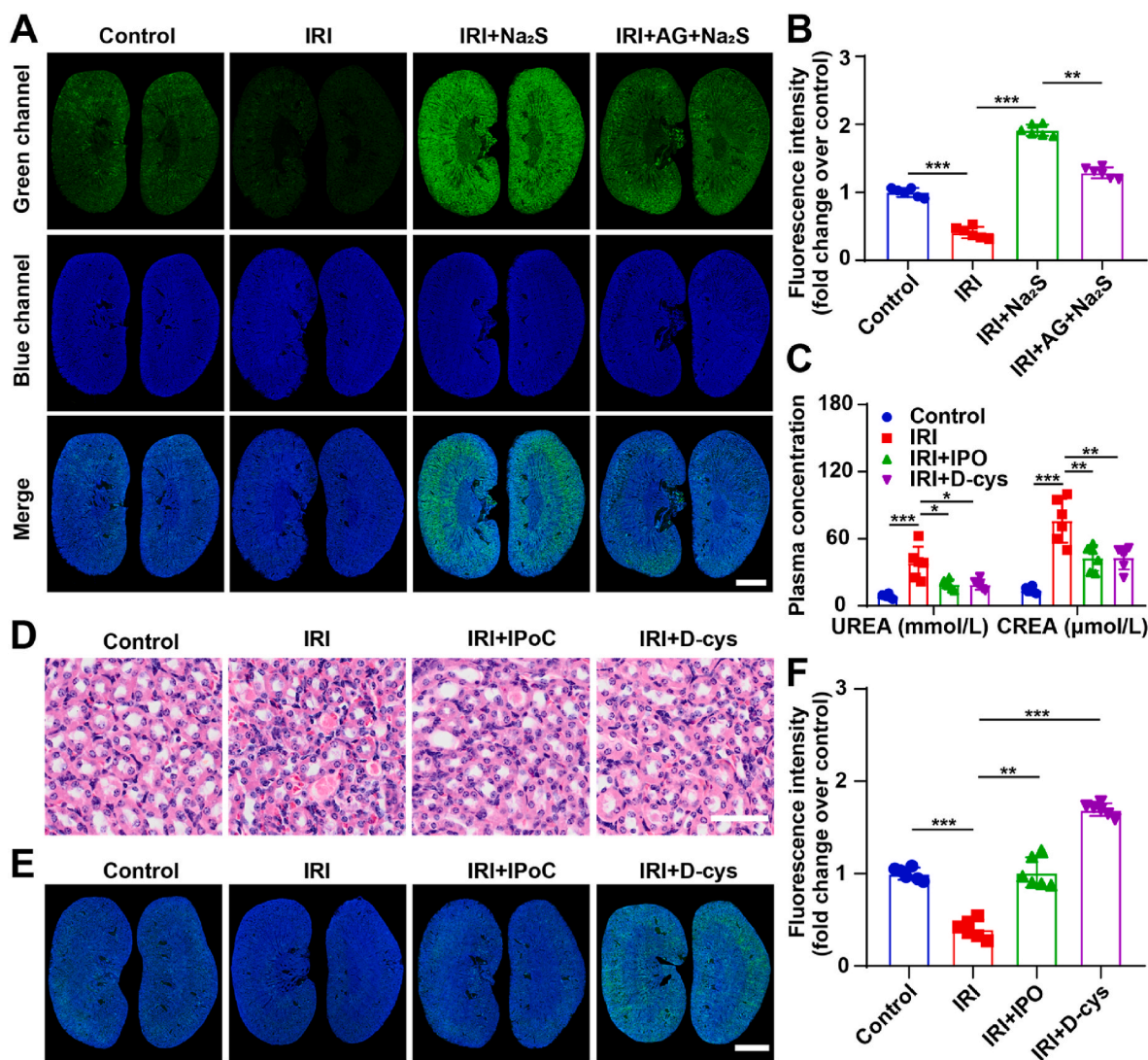

Fig. 5. (A) SNP-1-derived fluorescence showing the presence of HSNO in renal tissues of mice subjected to different treatments. Control, normal mice; IRI, mice with renal IRI; IRI + Na2S, mice with renal IRI and treated with 100 μg/kg Na2S; IRI + AG + Na2S, mice with renal IRI and pretreated with 2 mmol/kg AG followed by administration of 100 μg/kg Na2S. Scale bar, 2 mm. (B) Quantified fluorescence intensities. (C) Serum levels of UREA and CREA. (D) H&E-stained histological sections of renal tissues. Scale bar, 50 μm. (E) Fluorescence images indicate HSNO in renal tissues of mice. Scale bar, 2 mm. Control, normal mice; IRI, mice with renal IRI; IRI + IPoC, mice with renal IRI and treated with IPoC; IRI + D-cys: mice with IRI and treated with 8 mmol/kg D-cys. (F) Quantitative analysis of fluorescence intensities in various groups. Data are expressed as mean ± SD (n = 6). *$p < 0.05$, **$p < 0.01$, ***$p < 0.001$.

granulocyte infiltration, which were improved after 5-ASA treatment (Fig. 4E). Decreased colonic H_2S and NO levels, which meant lowered HSNO levels, were detected in 5-ASA-treated groups, compared with the control group (Figs. S20C–D). As expected, fluorescence intensities of SNP-1 were also weakened in the 5-ASA-treated groups (Fig. 4F and G). Additionally, a significant correlation between the fluorescence intensities of SNP-1 and DAI values (Spearman correlation coefficient r = 0.910, $p < 0.01$) was verified by correlation and regression analyses (Fig. S21). Together, these results demonstrated that the high HSNO level in colitis will be reduced with the remission of colonic injuries and the whole process can be monitored by using SNP-1. This further confirmed the advantage of SNP-1 for precise HSNO imaging. Moreover, HSNO can serve as a biomarker to diagnose and assess colitis, while SNP-1 is a promising fluorescent probe for this purpose.

3.5. Imaging of renal HSNO in mice suffering from renal ischemia/ reperfusion injury (IRI) using SNP-1

Subsequently, we examined whether SNP-1 probe can be applied to other HSNO-related pathological conditions. In this aspect, renal IRI was used, since H_2S and NO play a critical role in its pathogenesis and treatment [48–53]. We first tested SNP-1 as a HSNO detection method in renal tissues and observed increased green fluorescence in the HSNO-treated group (Fig. S22), confirmed the fluorescence response of SNP-1 to HSNO in renal tissues.

Next, we established a renal IRI model in mice using a previously reported method [32]. The fluorescence intensity of the IRI group decreased by 41% relative to the control group (Fig. 5A and B), indicating the down-regulated HSNO level in renal tissues injured by ischemia-reperfusion. Meanwhile, the H_2S level was found to be decreased in renal tissues in the IRI group compared with the normal control, although the corresponding NO levels increased (Figs. S23A–B). These findings are consistent with the previous result that renal ischemia-reperfusion leads to lowered H_2S levels [48,49,51] and elevated inducible nitric oxide synthase (iNOS) in kidneys [53,54]. On this basis, Na_2S was intraperitoneally injected to IRI mice to exogenously increase the H_2S level (Fig. S23A), thereby improving the HSNO level by the reaction between H_2S and NO. As expected, fluorescence of the IRI + Na_2S group was notably higher (by 1.92 times relative to control) than that of the IRI group, which could be partially suppressed by AG pre-treatment, since the NO level in the IRI + AG + Na_2S group was lower than that of the IRI + Na_2S group (Fig. S23B). Correspondingly, the fluorescence intensity observed in the IRI + AG + Na_2S group only increased 1.29 times relative to the control group (Fig. 5A and B). Together, the high sensitivity of SNP-1 to HSNO in biological systems was fully demonstrated, since decreased HSNO levels resulting from H_2S depletion in ischemia-reperfused kidneys [55] were accurately detected. Furthermore, only the increase of HSNO, but not the increase of NO alone, could improve the fluorescence intensity. These findings are in line with the in vitro results and adequately confirmed the high selectivity of SNP-1 to HSNO.

To further explore the response of SNP-1 to purely endogenous variation of HSNO contents, ischemic postconditioning (IPoC) [33] and D-cystine (D-cys) [31] were administrated to increase endogenous H_2S levels for the treatment of renal IRI [56,57]. Compared with the IRI model group, IPoC and D-cys treatment significantly reduced representative renal function indicators, including UREA and creatinine (CREA) (Fig. 5C). Additionally, histopathological analyses revealed that the IRI group exhibited damages mainly in the structure of renal tubules with the disordered arrangement, interstitial edema and hyperemia, necrotic tubules, casts formed from coagulated protein, and significant granulocyte infiltration, which were effectively alleviated in the IRI + IPoC and IRI + D-cys groups (Fig. 5D). Correspondingly, the fluorescence intensities of SNP-1 in the IRI + IPoC and IRI + D-cys groups were notably enhanced relative to the IRI group (Fig. 5E and F). In addition, the detected renal contents of H_2S and NO are consistent with the SNP-1

fluorescence intensities (Figs. S23C–D), since the HSNO levels in the IRI + IPoC and IRI + D-cys groups were higher than that of the IRI group. These results further demonstrated the effectiveness of our new fluorescent probe SNP-1 for HSNO detection through imaging, even when HSNO levels fluctuate during various treatments.

3.6. Safety studies

Finally, safety profiles of SNP-1 were examined. In vitro cytotoxicity tests in HepG2 cells showed relatively high cell viability at the tested concentrations up to 60 μM, indicating the good cytocompatibility of SNP-1 (Fig. S24). This result is in accordance with the previous report that this kind of phthalic anhydride derivatives are biocompatible at relatively low concentrations (<60 μM) [58,59]. Then, we evaluated the possible side effects of SNP-1 in mice after intravenous injection of SNP-1 at 50 mg/kg (five folds higher than the dose used for imaging studies in mice). Different analyses were performed at days 1 or 30 post injection for the short-term and long-term safety assessment, respectively. The results revealed no significant differences in body weight and major organ (heart, liver, spleen, lungs and kidneys) indices between the control and SNP-1 groups (Figs. S25A–B and S26A-B). Complete blood count showed normal hematological parameters for both groups. Quantificaiton of representative biomarkers relevant to hepatic and renal functions indicated that treatment with SNP-1 did not lead to notable hepato- and nephrotoxicities (Figs. S25C–J and S26C-J). Moreover, examination on histopathological sections revealed no necrosis, congestion, hemorrhage, or distinguishable inflammatory lesions in major organs (Figs. S27 and S28). Collectively, these results demonstrated that SNP-1 displayed good safety profile for intravenous injection.

4. Conclusion

In summary, we have designed and synthesized a novel fluorescence probe SNP-1 for visualizing and quantifying HSNO. SNP-1 displayed excellent fluorescence performance for HSNO detection, due to its rapid response, high selectivity, low detection limit, good quantum yield, and a broad linear range. Cellularly, SNP-1 could effectively image exogenous and endogenous HSNO in HepG2 cells. Furthermore, SNP-1 enabled successful fluorescence imaging of HSNO changes in acute ulcerative colitis and renal ischemia/reperfusion injury in mice. Importantly, SNP-1 demonstrated good safety performance. Consequently, HSNO displays high translational potential for diagnosis and therapeutic assessment of HSNO-associated diseases, such as colitis and ischemia-reperfusion in different organs. Moreover, SNP-1 can serve as a promising HSNO probe for both mechanistic studies and high-content drug screening.

Authorship contributions

Ning Zhang: Conceptualization, Methodology, Investigation, Formal analysis, Validation, Writing – original draft, Writing – review & editing, Visualization, Funding acquisition. Yifei Lu.: Investigation, Validation. Yong Huang: Investigation. Qing Zhang.: Investigation. Jianglin Tan.: Investigation. Jianxiang Zhang.: Conceptualization, Writing – review & editing, Supervision. Mengyun Yao.: Conceptualization, Methodology, Investigation, Validation, Writing – original draft, Writing – review & editing, Visualization, Funding acquisition. Gaoxing Luo.: Conceptualization, Resources, Writing – review & editing, Supervision, Funding acquisition.

Declaration of competing interest

The authors declare no conflict of interest.

Acknowledgements

Appendix A. Supplementary data

Supplementary data to this article can be found online at https://doi.org/10.1016/j.redox.2022.102372.

References

[1] M.M. Gadalla, S.H. Snyder, Hydrogen sulfide as a gasotransmitter, J. Neurochem. 113 (2010) 14–26.

[2] R. Hosoki, N. Matsuki, H. Kimura, The possible role of hydrogen sulfide as an endogenous smooth muscle relaxant in synergy with nitric oxide, Biochem. Biophys. Res. Commun. 237 (1997) 527–531.

[3] C. Coletta, A. Papapetropoulos, K. Erdelyi, G. Olah, K. Modis, P. Panopoulos, A. Asimakopoulou, D. Geroe, I. Sharina, E. Martin, C. Szabo, Hydrogen sulfide and nitric oxide are mutually dependent in the regulation of angiogenesis and endothelium-dependent vasorelaxation, Proc. Natl. Acad. Sci. U.S.A. 109 (2012) 9161–9166.

[4] C. Szabo, Gasotransmitters in cancer: from pathophysiology to experimental therapy, Nat. Rev. Drug Discov. 15 (2016) 185–203.

[5] M. Eberhardt, M. Dux, B. Namer, J. Miljkovic, N. Cordasic, C. Will, T.I. Kichko, J. de la Roche, M. Fischer, S.A. Suarez, D. Bikiel, K. Dorsch, A. Leffler, A. Babes, A. Lampert, J.K. Lennerz, J. Jacobi, M.A. Marti, F. Doctorovich, E.D. Hogestatt, P. M. Zygmunt, I. Ivanovic-Burmazovic, K. Messlinger, P. Reeh, M.R. Filipovic, H₂S and NO cooperatively regulate vascular tone by activating a neuroendocrine HNO-TRPA1-CGRP signalling pathway, Nat. Commun. 5 (2014) 4381.

[6] M. Whiteman, L. Li, I. Kostetski, S.H. Chu, J.L. Siau, M. Bhatia, P.K. Moore, Evidence for the formation of a novel nitrosothiol from the gaseous mediators nitric oxide and hydrogen sulphide, Biochem. Biophys. Res. Commun. 343 (2006) 303–310.

[7] M.Y. Ali, C.Y. Ping, Y.Y.P. Mok, L. Ling, M. Whiteman, M. Bhatia, P.K. Moore, Regulation of vascular nitric oxide in vitro and in vivo; a new role for endogenous hydrogen sulphide? Br. J. Pharmacol. 149 (2006) 625–634.

[8] J. Butler, J. Tanner, A.O. Oyekan, M.A. Yakubu, Does H₂S modulate NO level in cerebral microvascular cells? Faseb. J. 21 (2007): A1386-A1386.

[9] J.L. Kroll, C.A. Werchan, A.G. Reeves, K.J. Bruemmer, A.R. Lippert, T. Ritz, Sensitivity of salivary hydrogen sulfide to psychological stress and its association with exhaled nitric oxide and affect, Physiol. Behav. 179 (2017) 99–104.

[10] Y. Zhang, C. Tan, Q. Yang, H. Ye, X.-P. Chen, Arsenic phosphorus monolayer: a promising candidate for H₂S sensor and no degradation with high sensitivity and selectivity, IEEE Electron. Device Lett. 38 (2017) 1321–1324.

[11] G.-S. Oh, H.-O. Pae, B.-S. Lee, B.-N. Kim, J.-M. Kim, H.-R. Kim, S.B. Jeon, W. K. Jeon, H.-J. Chae, H.-T. Chung, Hydrogen sulfide inhibits nitric oxide production and nuclear factor-kappa B via heme oxygenase-1 expression in RAW264.7 macrophages stimulated with lipopolysaccharide, Free Radic. Biol. Med. 41 (2006) 106–119.

[12] C.E. Cooper, G.C. Brown, The inhibition of mitochondrial cytochrome oxidase by the gases carbon monoxide, nitric oxide, hydrogen cyanide and hydrogen sulfide: chemical mechanism and physiological significance, J. Bioenerg. Biomembr. 40 (2008) 533–539.

[13] J.P. Marcolongo, M.F. Venancio, W.R. Rocha, F. Doctorovich, J.A. Olabe, NO/H₂S "crosstalk" reactions. The role of thionitrites (SNO-) and perthionitrites (SSNO-), Inorg. Chem. 58 (2019) 14981–14997.

[14] J. Miljkovic, I. Ivanovic-Burmazovic, M. Filipovic, H₂S generates HNO and HSNO from nitrite by a heme iron-catalyzed metabolism in mitochondria, Free Radic. Biol. Med. 65 (2013). S98-S98.

[15] M.R. Filipovic, J.L. Miljkovic, T. Nauser, M. Royzen, K. Klos, T. Shubina, W. H. Koppenol, S.J. Lippard, I. Ivanovic-Burmazovic, Chemical characterization of the smallest S-nitrosothiol, HSNO; cellular cross-talk of H2S and S-nitrosothiols, J. Am. Chem. Soc. 134 (2012) 12016–12027.

[16] M. Nava, M.-A. Martin-Drumel, C.A. Lopez, K.N. Crabtree, C.C. Womack, T. L. Nguyen, S. Thorwirth, C.C. Cummins, J.F. Stanton, M.C. McCarthy, Spontaneous and selective formation of HSNO, a crucial intermediate linking H₂S and nitroso chemistries, J. Am. Chem. Soc. 138 (2016) 11441–11444.

[17] X. Zhang, L. Zhang, M. Gao, Y. Wang, L. Chen, A near-infrared fluorescent probe for observing thionitrous acid-mediated hydrogen polysulfides formation and fluctuation in cells and in vivo under hypoxia stress, J. Hazard Mater. (2020) 396.

[18] I. Ivanovic-Burmazovic, M.R. Filipovic, Saying no to H₂S: a story of HNO, HSNO, and SSNO, Inorg. Chem. 58 (2019) 4039–4051.

[19] C.-H. Lai, E.Y. Li, P.-T. Chou, Isomerization reactions of RSNO (R=H, CnH2n+1 n <= 4), Theor. Chem. Acc. 117 (2007) 145–152.

[20] Q.K. Timerghazin, G.H. Peslherbe, A.M. English, Structure and stability of HSNO, the simplest S-nitrosothiol, Phys. Chem. Chem. Phys. 10 (2008) 1532–1539.

[21] Q.K. Timerghazin, A.M. English, G.H. Peslherbe, On the multireference character of S-nitrosothiols: a theoretical study of HSNO, Chem. Phys. Lett. 454 (2008) 24–29.

[22] N. Lau, M.D. Pluth, Reactive sulfur species (RSS): persulfides, polysulfides, potential, and problems, Curr. Opin. Chem. Biol. 49 (2019) 1–8.

[23] W. Chen, T. Matsunaga, D.L. Neill, C.-t. Yang, T. Akaike, M. Xian, Rational design of a dual-reactivity-based fluorescent probe for visualizing intracellular HSNO, Angew. Chem., Int. Ed. 58 (2019) 16067–16070.

[24] R. Fazaeli, M. Solimannejad, A. Seif, Analysis of torsional barrier height of HSNO as the simplest S-nitrosothiol, J. Chem. Sci. 125 (2013) 913–917.

[25] R. Wedmann, A. Zahl, T.E. Shubina, M. Duerr, F.W. Heinemann, B.E. C. Bugenhagen, P. Burger, I. Ivanovic-Burmazovic, M.R. Filipovic, Does perthionitrite (SSNO-) account for sustained bioactivity of no? A (Bio)chemical characterization, Inorg. Chem. 54 (2015) 9367–9380.

[26] T. Nagano, T. Yoshimura, Bioimaging of nitric oxide, Chem. Rev. 102 (2002) 1235–1269.

[27] X.Q. Chen, T. Pradhan, F. Wang, J.S. Kim, J. Yoon, Fluorescent chemosensors based on spiroring-opening of xanthenes and related derivatives, Chem. Rev. 112 (2012) 1910–1956.

[28] Y. Tian, F. Xin, J. Jing, X. Zhang, Fluorescence imaging of lysosomal hydrogen selenide under oxygen-controlled conditions, J. Mater. Chem. B 7 (2019) 2829–2834.

[29] S. Wirtz, V. Popp, M. Kindermann, K. Gerlach, B. Weigmann, S. Fichtner-Feigl, M. F. Neurath, Chemically induced mouse models of acute and chronic intestinal inflammation, Nat. Protoc. 12 (2017) 1295–1309.

[30] C. Li, Y. Zhao, J. Cheng, J. Guo, Q. Zhang, X. Zhang, J. Ren, F. Wang, J. Huang, H. Hu, R. Wang, J. Zhang, A proresolving peptide nanotherapy for site-specific treatment of inflammatory bowel disease by regulating proinflammatory microenvironment and gut microbiota, Adv. Sci. 6 (2019), 1900610.

[31] N. Shibuya, S. Koike, M. Tanaka, M. Ishigami-Yuasa, Y. Kimura, Y. Ogasawara, K. Fukui, N. Nagahara, H. Kimura, A novel pathway for the production of hydrogen sulfide from D-cysteine in mammalian cells, Nat. Commun. 4 (2013) 1366.

[32] E.E. Hesketh, A. Czopek, M. Clay, G. Borthwick, D. Ferenbach, D. Kluth, J. Hughes, Renal ischaemia reperfusion injury: a mouse model of injury and regeneration, Jove-J. Vis. Exp. 88 (2014), e51816.

[33] Y. Tian, J. Shu, R. Huang, X. Chu, X. Mei, Protective effect of renal ischemic postconditioning in renal ischemic-reperfusion injury, Transl. Androl. Urol. 9 (2020) 1356–1365.

[34] C.L. Bianco, T.A. Chavez, V. Sosa, S.S. Saund, Q.N.N. Nguyen, D.J. Tantillo, A. S. Ichimura, J.P. Toscano, J.M. Fukuto, The chemical biology of the persulfide (RSSH)/perthiyl (RSS center dot) redox couple and possible role in biological redox signaling, Free Radic. Biol. Med. 101 (2016) 20–31.

[35] A.S. Stroppel, M. Paolillo, T. Ziegler, R. Feil, T. Stafforst, Npom-protected NONOate enables light-triggered NO/cGMP signalling in primary vascular smooth muscle cells, Chembiochem 19 (2018) 1312–1318.

[36] A. Feechan, E. Kwon, B.W. Yun, Y.Q. Wang, J.A. Pallas, G.J. Loake, A central role for S-nitrosothiols in plant disease resistance, Proc. Natl. Acad. Sci. U.S.A. 102 (2005) 8054–8059.

[37] M.A. Rahman, B.M. Cumming, K.W. Addicott, H.T. Pacl, S.L. Russell, K. Nargan, T. Naidoo, P.K. Ramdial, J.H. Adamson, R. Wang, A.J.C. Steyn, Hydrogen sulfide dysregulates the immune response by suppressing central carbon metabolism to promote tuberculosis, Proc. Natl. Acad. Sci. U.S.A. 117 (2020) 6663–6674.

[38] P.-H. Feng, K.-Y. Lee, Y.-L. Chang, Y.-F. Chan, L.-W. Kuo, T.-Y. Lin, F.-T. Chung, C.-S. Kuo, C.-T. Yu, S.-M. Lin, C.-H. Wang, C.-L. Chou, C.-D. Huang, H.-P. Kuo, CD14(+)S100A9(+) monocytic myeloid-derived suppressor cells and their clinical relevance in non-small cell lung cancer, Am. J. Respir. Crit. Care Med. 186 (2012) 1025–1036.

[39] R. Yang, C. Qu, Y. Zhou, J.E. Konkel, S. Shi, Y. Liu, C. Chen, S. Liu, D. Liu, Y. Chen, E. Zandi, W. Chen, Y. Zhou, S. Shi, Hydrogen sulfide promotes tet1 and tet2-mediated Foxp3 demethylation to drive regulatory T cell differentiation and maintain immune homeostasis, Immunity 43 (2015) 251–263.

[40] W.E.W. Roediger, Review article: nitric oxide from dysbiotic bacterial respiration of nitrate in the pathogenesis and as a target for therapy of ulcerative colitis, Aliment. Pharmacol. Ther. 27 (2008) 531–541.

[41] J. Levine, C.J. Ellis, J.K. Furne, J. Springfield, M.D. Levitt, Fecal hydrogen sulfide production in ulcerative colitis, Am. J. Gastroenterol. 93 (1998) 83–87.

[42] S. Ramasamy, S. Singh, P. Taniere, M.J. Langman, M.C. Eggo, Sulfide-detoxifying enzymes in the human colon are decreased in cancer and upregulated in differentiation, Am. J. Physiol. Gastrointest. Liver Physiol. 291 (2006) G288–G296.

[43] P.D. Reynolds, S.J. Middleton, G.M. Hansford, J.O. Hunter, Confirmation of nitric oxide synthesis in active ulcerative colitis by infra-red diode laser spectroscopy, Eur. J. Gastroenterol. Hepatol. 9 (1997) 463–466.

[44] C.A. Lamb, N.A. Kennedy, T. Raine, P.A. Hendy, P.J. Smith, J.K. Limdi, B.H. Hayee, M.C.E. Lomer, G.C. Parkes, C. Selinger, K.J. Barrett, R.J. Davies, C. Bennett, S. Gittens, M.G. Dunlop, O. Faiz, A. Fraser, V. Garrick, P.D. Johnston, M. Parkes, J. Sanderson, H. Terry, D.R. Gaya, T.H. Iqbal, S.A. Taylor, M. Smith, M. Brookes, R. Hansen, A.B. Hawthorne, I.B.D.G.e.C. G, British Society of Gastroenterology consensus guidelines on the management of inflammatory bowel disease in adults, Gut 68 (2019) S1–S106.

[45] S. Singh, J.D. Feuerstein, D.G. Binion, W.J. Tremaine, AGA technical review on the management of mild-to-moderate ulcerative colitis, Gastroenterology 156 (2019) 769.

[46] Y. You, J.-J. Fu, J. Meng, G.-D. Huang, Y.-H. Liu, Effect of N-acetylcysteine on the murine model of colitis induced by dextran sodium sulfate through up-regulating PON1 activity, Dig. Dis. Sci. 54 (2009) 1643–1650.

[47] X. Wang, Y. Sun, Y. Zhao, Y. Ding, X. Zhang, L. Kong, Z. Li, Q. Guo, L. Zhao, Oroxyloside prevents dextran sulfate sodium-induced experimental colitis in mice by inhibiting NF-kappa B pathway through PPAR gamma activation, Biochem. Pharmacol. 106 (2016) 70–81.

[48] O. Karmin, Y.L. Siow, Metabolic imbalance of homocysteine and hydrogen sulfide in kidney disease, Curr. Med. Chem. 25 (2018) 367–377.

[49] C.K. Nicholson, J.W. Calvert, Hydrogen sulfide and ischemia-reperfusion injury, Pharmacol. Res. 62 (2010) 289–297.

[50] A. Hosszu, Z. Antal, L. Lenart, J. Hodrea, S. Koszegi, D.B. Balogh, N.F. Banki, L. Wagner, A. Denes, P. Hamar, P. Degrell, A. Vannay, A.J. Szabo, A. Fekete, Sigma 1-receptor agonism protects against renal ischemia-reperfusion injury, J. Am. Soc. Nephrol. 28 (2017) 152–165.

[51] J.C. Pieretti, C.V. Cruz Junho, M.S. Carneiro-Ramos, A.B. Seabra, H₂S- and NO-releasing gasotransmitter platform: a crosstalk signaling pathway in the treatment of acute kidney injury, Pharmacol. Res. 161 (2020), 105121.

[52] P. Tripatara, N.S.A. Patel, A. Webb, K. Rathod, F.M.J. Lecomte, E. Mazzon, S. Cuzzocrea, M.M. Yaqoob, A. Ahluwalia, C. Thiemermann, Nitrite-derived nitric oxide protects the rat kidney against ischemia/reperfusion injury in vivo: role for xanthine oxidoreductase, J. Am. Soc. Nephrol. 18 (2007) 570–580.

[53] P. Wang, Q. Zhu, N. Wu, Y.L. Siow, H. Aukema, O. Karmin, Tyrosol attenuates ischemia-reperfusion-induced kidney injury via inhibition of inducible nitric oxide synthase, J. Agric. Food Chem. 61 (2013) 3669–3675.

[54] M. Okamoto, K. Tsuchiya, Y. Kanematsu, Y. Izawa, M. Yoshizumi, S. Kagawa, T. Tamaki, Nitrite-derived nitric oxide formation following ischemia-reperfusion injury in kidney, Am. J. Physiology-Renal. 288 (2005) F182–F187.

[55] J. Ni, L. Jiang, G. Shen, Z. Xia, L. Zhang, J. Xu, Q. Feng, H. Qu, F. Xu, X. Li, Hydrogen sulfide reduces pyroptosis and alleviates ischemia-reperfusion-induced acute kidney injury by inhibiting NLRP3 inflammasome, Life Sci. 284 (2021), 119466.

[56] Y. Chen, L. Zhao, S. Jiang, Z. Hu, B. Hu, F. Tong, R. Shen, Cystathionine gamma-lyase is involved in the renoprotective effect of brief and repeated ischemic postconditioning after renal ischemia/reperfusion injury in diabetes mellitus, Transplant. Proc. 50 (2018) 1549–1557.

[57] H. Kimura, The physiological role of hydrogen sulfide and beyond, Nitric Oxide-Biol. Ch. 41 (2014) 4–10.

[58] N. Zhang, P. Hu, Y. Wang, Q. Tang, Q. Zheng, Z. Wang, Y. He, A reactive oxygen species (ROS) activated hydrogen sulfide (H₂S) donor with self-reporting fluorescence, ACS Sens. 5 (2020) 319–326.

[59] M. Yao, Y. Lu, L. Shi, Y. Huang, Q. Zhang, J. Tan, P. Hu, J. Zhang, G. Luo, N. Zhang, A ROS-responsive, self-immolative and self-reporting hydrogen sulfide donor with multiple biological activities for the treatment of myocardial infarction, Bioact. Mater. 9 (2022) 168–182.